Lightweight, superelastic boron nitride/polydimethylsiloxane foam as air dielectric substitute for multifunctional capacitive sensor applications

Tay, Roland Yingjie; Li, Hongling; Lin, Jinjun; Wang, Hong; Lim, Jacob Song Kiat; Chen, Shuai; Leong, Wei Lin; Tsang, Siu Hon; Teo, Edwin Hang Tong

2020

Tay, R. Y., Li, H., Lin, J., Wang, H., Lim, J. S. K., Chen, S., . . . Teo, E. H. T. (2020). Lightweight, superelastic boron nitride/polydimethylsiloxane foam as air dielectric substitute for multifunctional capacitive sensor applications. Advanced Functional Materials, 30(10), 1909604-. doi:10.1002/adfm.201909604

https://hdl.handle.net/10356/138867

https://doi.org/10.1002/adfm.201909604

DOI: 10.1002/ ((please add manuscript number))
Article type: Full Paper

Lightweight, Superelastic Boron Nitride/Polydimethylsiloxane Foam as Air Dielectric Substitute for Multifunctional Capacitive Sensor Applications

*Roland Yingjie Tay, Hongling Li, Jinjun Lin, Hong Wang, Jacob Song Kiat Lim, Shuai Chen, Wei Lin Leong, Siu Hon Tsang, and Edwin Hang Tong Teo**

Dr. R. Y. Tay, Dr. H. Li, J. Lin, Dr. H. Wang, Dr. S. Chen, Prof. W. L. Leong, Prof. E. H. T. Teo
School of Electrical and Electronic Engineering, Nanyang Technological University, 50 Nanyang Avenue, Singapore 639798, Singapore
E-mail: htteo@ntu.edu.sg

Dr. R. Y. Tay, J. S. K. Lim, Dr. S. H. Tsang
Temasek Laboratories@NTU, 50 Nanyang Avenue, Singapore 639798, Singapore

J. S. K. Lim, Prof. E. H. T. Teo
School of Materials Science and Engineering, Nanyang Technological University, 50 Nanyang Avenue, Singapore 639798, Singapore

R. Y. T. and H. L. contributed equally to this work.

Keywords: Boron nitride, porous polydimethylsiloxane, lightweight, superelastic, multifunctional sensor

Porous polymeric foams as dielectric layer for highly sensitive capacitive based pressure sensors have been extensively explored owing to their excellent flexibility and elasticity. Despite intensive efforts, most of the previously reported porous polymer foams still suffer from the difficulty in further lowering the attainable density limit of ~0.1 g/cm^3 while retaining high sensitivity and compressibility due to the limitations on existing fabrication techniques and materials. Herein, utilizing three-dimensional interconnected networks of few-layer hexagonal boron nitride foams (*h*-BNFs) as supporting frameworks, lightweight and highly porous BN/polydimethylsiloxane composite foams (BNF@PDMS) with densities reaching as low as 15 mg/cm^3 and permittivity close to that of air were fabricated. To the best of our knowledge, this is the lightest PDMS-based foams to date. Owing to the synergistic effects between BN and PDMS, these lightweight composite foams possess excellent

mechanical resilience, extremely high compressibility (up to 95% strain), good cyclic performance and superelasticity. Being electrically non-conductive, the potential application of BNF@PDMS as a dielectric layer for capacitive sensor was further demonstrated. Remarkably, the as-fabricated device could perform multiple sensing functions such as non-contact touch sensor, environmental monitoring sensor and high sensitivity pressure sensor that could detect extremely low pressures of below 1 Pa.

1. Introduction

Over the last decades, there is an unprecedented growth in demand for pressure sensors as compelled by necessity for their application in many of today's technologies. They provide real-time information that are conceived by changing their properties in response to external mechanical stimuli. Ranging from our familiar smart devices with touch-screen capabilities to more sophisticated systems such as electronic skins for robotics, smart prosthesis, biomedical and healthcare monitoring devices,[1] incorporation of pressure sensors is integral. In general, the working principle for sensors can be classified into capacitive,[2] piezoresistive,[3] piezoelectric[4], triboelectric[5] and optical.[6] Particularly, capacitive sensors exhibit several advantages such as simplicity and ease of fabrication, low power consumption, stable with good repeatability, high sensitivity and fast response time.[7] A parallel-plate capacitive sensor is composed of a dielectric layer sandwiched in between two conducting electrode plates and detects changes to its capacitance as defined by $C = \varepsilon_0 \varepsilon_r \frac{A}{d}$, where ε_0 and ε_r is the permittivity

of vacuum and dielectric layer, respectively, A is the overlapped area and d is the distance between the two electrodes plates. Although increasing the contact area of the electrodes by means of micro-patterning and using nanostructured materials can improve the overall sensitivity of the device,[8] the more important component of the sensor lies within the variability of the dielectric layer where substantial changes can be conceived through varying

both its permittivity and compressibility.[7a, 7b, 9] Moreover, it could also potentially respond to a variety of stimuli thus enabling multi-functionality.

Although various polymeric foams such as acrylates,[10] polyolefin[11] and polyurethane[12] have been used as dielectric layers for capacitive sensors, polydimethylsiloxane (PDMS) based foams are by far the most prevalent owing to their commercial availability, excellent flexibility and elasticity, mechanical toughness and bio-compatibility.[7a, 7b, 8c, 9, 13] Specifically, controlling the porosity or air gaps within these polymeric foams is key to achieve high compressibility and sensitivity of the capacitive pressure sensor device. To date, several strategies have been utilized to accomplish this purpose. For instance, micro-structured or porous PDMS can be fabricated by casting onto pre-patterned moulds,[7a, 8b, 9, 14] using sacrificial hard templates (e.g., sugar cubes,[15] salt crystals,[16] citric acid monohydrate,[17] polystyrene beads,[13a] and metal foams,[18]), gas foaming,[13b, 19] and emulsion templating.[20] Among them, PDMS foams prepared by choosing highly porous Ni foams as templates were demonstrated to exhibit the lowest density of ~0.1 g/cm^3 (~10 times lighter than solid PDMS) because of the relatively large pore size (few hundreds of microns) and interconnected structure of Ni foams which allow coating of diluted PDMS.[18a, 18c, 21] Despite these efforts, it is still difficult to further lower the attainable density limit of porous PDMS foams due to the techniques available and the physical properties of PDMS.

To address these limitations, in this work, by utilizing three-dimensional (3D) interconnected networks of few-layer hexagonal boron nitride foams (*h*-BNFs) as supporting frameworks, porous BN/PDMS composite foams (BNF@PDMS) with densities as low as 15 mg/cm^3 were achieved. Being well-known for many unique and impressive properties including high thermal conductivity[22] and mechanical strength,[23] chemically inert and resistant to oxidation,[24] electrically non-conducting as well as bio-compatible,[25] BN is an ideal material of choice to be integrated as a dielectric layer. Synergizing in perfect unison

with PDMS, the as-prepared BNF@PDMS composites with ultralow density exhibit exceptional mechanical resilience, extremely high compressibility (up to 95%) with superelastic properties and stable cyclic performance. Because of their extremely high porosity (> 98%), they also display ultralow permittivity almost comparable to that of air. As such, the BNF@PDMS was further served as a dielectric layer for capacitive sensing applications. Impressively, the as-fabricated sensor device showed multifunctional sensing capabilities such as non-contact touch, environmental monitoring and high sensitivity pressure sensors.

2. Results and Discussion

2.1. Fabrication and Structural Characterization of BNF@PDMS

Figure 1a shows the schematic of the fabrication process of BNF@PDMS (details in the experimental section). In brief, commercially available Ni foams with more than 95% porosity were used as templates and few-layer *h*-BN was grown on the surface of the Ni struts using chemical vapor deposition (CVD) method.[26] The as-grown BN/Ni foam was then soaked in diluted PDMS solution (3 – 10 wt%) for an hour to ensure conformal coating and was left to dry overnight. Although the BN/Ni foam is significantly more hydrophobic than bare Ni foam, both of the foams are superoleophilic and are easily wetted by *n*-hexane (Figure S1, Supporting Information), suggesting that the PDMS in *n*-hexane solution is easily penetrated and absorbed by the foam which enabled homogenous coating. Finally, the sacrificial Ni foam template was removed by etching in diluted hydrochloric acid. The resulting BNF@PDMS exhibit excellent mechanical resilience as shown in Figure 1b. No detrimental damage to the foams was observed when common deformations such as bending, twisting and rolling were performed and all the foams returned to their respective original form upon load releasing.

By varying the concentration of PDMS in the coating solution, BNF@PDMS with densities reaching as low as ~15 mg/cm^3 and having a corresponding porosity of > 98% can be achieved (Table S1, Supporting Information). Remarkably, this value is the lightest among previously reported PDMS foams and close to that of graphene and BN based aerogels (Table S2, Supporting Information). It should be mentioned that some of the pores were covered with PDMS when higher concentrations of PDMS solutions were used (Figure S2, Supporting Information). To better understand the crucial role of the BN layer in order to achieving such lightweight low-density foam, the morphology and microstructure of BNFs were further characterized by scanning and transmission electron microscopies (SEM and TEM, Figure 1c–f). It is observed that the freestanding BN foam retains the macroporous structure of the Ni foam template (Figure 1c) and possesses a very low density of ~0.9 mg/cm^3. It is also found that the deposited BN is typically composed of few-layer (< 10 layers) with an interlayer spacing of ~0.34 nm, as identified by the TEM images taken at the edges of a BN sheet (Figure 1d,e). Figure 1f shows the atomic resolution TEM image taken within the interior of the BN sheet and its corresponding fast Fourier transform (FFT) revealed a distinct hexagonal structure consistent with *h*-BN.

Hence, having a continuous structure and being able to be freestanding by its own, the few-layer BN foam provides a structural frame which is rigid enough to provide support for the PDMS coating. In contrast, when bare Ni foam was used as the template at a lower concentration of PDMS coating solution, the resulting PDMS foam was observed to have uneven struts and the entire structure collapsed after the removal of the Ni (Figure S3 and S4, Supporting Information), which is attributed to the high value of the work of adhesion and the low bending stiffness of the PDMS coating layer.[27] On the other hand, the few-layer *h*-BN act as an interfacial barrier along the inner surface of the tubular hollow PDMS walls and thereby reduces the work of adhesion and provides additional support which enhances the

bending stiffness of the PDMS layer. These effectively prevents the sticking of PDMS within the hollow walls and buckling which causes the PDMS foam to collapse. The typical SEM image of BNF@PDMS and its corresponding elemental mappings are presented in Figure 1g. It is observed that the BNF@PDMS also preserved the same macroporous morphology with the BN/Ni foam (Figure S5, Supporting Information). In addition, all the elements (B and N from BN foam and C, Si, O from PDMS) are observed to be homogenously distributed along the cellular networks of the foam as identified by the energy dispersive X-ray (EDX) mappings, further confirming the conformal coating of the diluted PDMS on the BNF.

The microstructure and thermal stability of the as-prepared BNF@PDMS were further characterized using Raman spectroscopy and thermogravimetric analysis (TGA). Figure 2a shows the comparison of the Raman spectra for pure BNF, pure PDMS foam and BNF@PDMS. For pure BNF, a characteristic peak located at ~1367 cm^{-1} is attributed to E_{2g} vibration mode of *h*-BN.[28] The PDMS foam exhibits four peaks centered at ~1261, ~1411, ~2906, ~2963 cm^{-1} which are assigned to the symmetric and asymmetric vibrations of CH_3.[29] For the BNF@PDMS, all of these five characteristic peaks can be observed. Figure 2b shows the deconvolution of *h*-BN peak at ~1367 cm^{-1} and PDMS peaks at ~1262 and ~1410 cm^{-1}, respectively, indicating the successful integration of PDMS coating on BN without changing both of their microstructures. The thermal stability and BN content of the BNF@PDMS were further evaluated by TGA under air as shown in Figure 2c. For pure BNF, negligible weight loss was found when the temperature is below ~900 °C, while a slight gain in weight was observed at ~900 °C, attributing to oxidation of BN into B_2O_3. For pure PDMS foam, thermal decomposition begins at ~300 °C with a total weight loss of 30.3% at 800 °C. The thermal decomposition of BNF@PDMS also begins at ~300 °C but has a lower weight loss of 24.2% due to the presence of BN. From the difference in weight loss, the extracted BN content was

6.1% which has an equivalent density of ~0.93 mg/cm^3, in consistent with our measurements on pure BNF.

2.2. Mechanical Characterization of BNF@PDMS

To further evaluate the mechanical properties of the BNF@PDMS foams, uniaxial compression tests were systematically conducted. Figure 3a displays the compressive stress (σ) – strain (ε) curves for the BNF@PDMS with different densities at a strain amplitude of 80%. It can be observed that all the foams displayed full recovery after compression with their maximum stress (σ_M) increases with increasing foam density. The foam with different density is denoted as BNF@PDMS-x, where x is the density of the foam in mg/cm^3. The superelastic properties of the foam with the lowest density, BNF@PDMS-15, was further characterized to determine the extent of its mechanical resilience to compression. Figure 3b shows the σ–ε curves of 6 compression cycles with strain amplitudes of 20, 40, 60, 80, 90 and 95% in successive sequence. It is evident that each successive loading curve thread at the maximum stress of the preceding curve, demonstrating a perfect strain memory effect with no residual deformation over the entire range of our measurements.

Further cyclic compression tests were performed on the BNF@PDMS-15 as shown in Figure 3c. From the loading curves in each cycle, three deformation regimes were observed which are typical to those of open cell foams.[18c, 26] An initial Hookean region at $\varepsilon < 5\%$ attributed to bending of the tubular cells, followed by a plateau at $5\% < \varepsilon < 60\%$ arising from postbuckling deformations of the branches and nodes of the interconnected structure and a final densification at $\varepsilon > 60\%$ with a rapidly increasing σ caused by the increase in frictional contacts and collisions between tubular walls.[18c, 26, 30] The BNF@PDMS-15 exhibits full recovery even after 10 compression cycles at 80% strain amplitude, as evidenced from its unloading curves where the σ decreases rapidly to about 70% strain but does not entirely

vanish until ε returns to zero. Figure 3d shows the summary plots of the derived energy loss coefficients ($\Delta U/U$), maximum compressive stress (σ_M), and elastic modulus (E) extracted from the 10 compression cycles. During the prime cycle at 80% strain amplitude, the $\Delta U/U$ was ~0.7 and decreased considerably during the next two cycles to ~0.53 where it begins to stabilize and was measured at 0.46 at the 10th cycle. A similar trend can be observed for both the σ_M and E where they diminish with increasing cycles. Remarkably, it possessed a very low σ_M of 1.86 kPa for the 1st cycle and 1.52 kPa for the 10th, and E of 4.12 kPa for the 1st cycle and 1.64 kPa for the 10th, all of which are among the lowest as compared to other foam-like materials (Table S2, Supporting Information).

2.3. Dielectric Properties of BNF@PDMS

Being mechanically resilient yet highly compressible and electrically non-conductive, BNF@PDMS is expected to have great potential as a dielectric layer for capacitive sensing applications. As such, its dielectric properties in response to varying strains were further evaluated by using a variable parallel-plate capacitor controlled by a micromanipulator. Figure 4a shows the plots of the dielectric constant relative to air (k/k_{air}) and loss tangent (tan δ) as a function of frequency of the various BNF@PDMS with different densities under unstrained condition. Due to the high porosity, all the BNF@PDMS exhibit ultralow permittivity which was stable over the measured frequency range of 10 KHz – 2 MHz. Their corresponding k/k_{air} measured at 1 MHz was 1.018 for BNF@PDMS-15, 1.037 for BNF@PDMS-30 and 1.057 for BNF@PDMS-50 with a low tan δ not exceeding 0.005. The increment in k/k_{air} with increasing foam density is reasonable because the dielectric constants for BN and PDMS are ~2 – 4[31] and ~2.3 – 2.8,[32] respectively.

Figure 4b shows the change in capacitance ($\Delta C/C_0$) as a function of compressive strain at 1 MHz for BNF@PDMS in comparison to air and pure BNF. The measured capacitance *vs.*

distance plot is given in Figure S6, Supporting Information. It is observed that the $\Delta C/C_0$ of all the foams behaved similar to air which increases almost proportionally to the reciprocal of the distance. The corresponding extracted k/k_{air} as a function of compressive strain in presented in Figure 4c. As expected, k/k_{air} increases with increasing compressive strain due to the increase in volume density. For pure BNF, the measured k/k_{air} under zero compressive strain is 1.01 and increases to 1.03 when compressed at 90% strain. The slight deviation of these values from a previous report[26] is possibly due to a lower foam density of ~0.9 mg/cm^3 as compared to that of reported BNF. As for BNF@PDMS-15, the k/k_{air} increases slightly from 1.02 at zero strain to 1.04 at 60% strain and increases more steeply to 1.10 at 90% strain. The steep increase which starts at ~60% strain is attributed to the densification of the foam which is consistent with our uniaxial compression measurements in Figure 3. BNF@PDMS-30 and 50 showed a similar trend but with a higher and slightly steeper increase in k/k_{air} which reaches saturation at 86.8% and 84.2% strain, respectively.

To ensure the repeatable performance of the BNF@PDMS, further cyclic compression tests were conducted. Figure 4d shows the evolution of k/k_{air} during the first compression cycle for BNF@PDMS-15 at 90% strain. It is observed that the change in k/k_{air} remained consistent over the course of the loading and unloading cycle. Repeated cyclic experiments of up to 10 compression cycles at 90% strain had also confirmed that the response of the dielectric property of the BNF@PDMS remained highly reproducible (inset of Figure 4d) with an identical trend in k/k_{air} as a function of strain during the 1st and 10th compression cycle (Figure S7, Supporting Information).

2.4. Multifunctional Capacitive Sensor

To demonstrate the potential of the BNF@PDMS as a dielectric layer for capacitive sensors, a parallel-plate capacitor was fabricated using indium tin oxide coated polyethylene

terephthalate films (ITO/PETs) as the conducting electrodes and BNF@PDMS as the dielectric layer, as shown in the photograph and schematic in Figure 5a. It is observed that the capacitance of this device responded to several stimuli. In these sets of experiments, the $\Delta C/C_0$ as a function of time was recorded with various stimulations performed to the device. As observed in Figure 5b, the device operated as a non-contact touch sensor where the capacitance decreases when an object approaches the device at close proximity. Interestingly, when a finger and a tweezer were alternately hovered close to the capacitor, it is apparent that the $\Delta C/C_0$ varies with the size of the object. When the finger is placed above the device, a decrease in $\Delta C/C_0$ is ~2% (in red), while a lower value of ~1.5% (in blue) is observed for the tweezer with a smaller size. This reduction in capacitance is caused by the absorption of fringing electric field that resides within the dielectric layer. Relative to the size and distance of the approaching object, parts of the fringing electric field will be absorbed, resulting in the variation of $\Delta C/C_0$.[1c, 33]

Owing to its extremely low density with a corresponding porosity of > 98%, the overall dielectric constant of the as-fabricated BNF@PDMS is almost comparable to that of air. This unique property makes it an ideal substitute for air dielectric which could also be used to detect small changes in the environment. Figure 5c shows the $\Delta C/C_0$ by gently blowing through the device. As human breath contains higher amount of water vapor relative to the air in the laboratory, the permittivity of the foam increases when the water vapor fills up the air pockets in the foam (k_{water} ~80), leading to a ~2.5% increase in $\Delta C/C_0$ for our device. Over time, the water vapor diffuses out of the foam and its permittivity will be restored back close to that of air. Hence, such porous foams are expected to be a feasible solid-state replacement for air dielectric used in humidity[34] and smoke detection[35] sensor applications.

The lightweight BNF@PDMS with high compressibility also holds great promise as a dielectric layer for high sensitivity pressure sensing applications. Figure 5d shows the $\Delta C/C_0$

in response to pressing the device with a tweezer. It is noted that the approaching tweezer caused an initial dip to the capacitance (~-1.5%) and a sudden spike occurs when the tweezer is pressed onto the device (inset of Figure 5d). The magnitude of the $\Delta C/C_0$ is determined by the intensity of the "press" which compresses the BNF@PDMS and thereby narrows the distance between the two electrodes thus increasing its capacitance. Upon load releasing, the compressed BNF@PDMS recovers back to its original shape and the capacitance returned to C_0. Figure 5e shows the $\Delta C/C_0$ values by loading a total of four flower petals (~13 – 14 mg per petal) in successive sequence. It should be mentioned that the observable decrease in $\Delta C/C_0$ is caused by the approaching tweezer. Remarkably, a $\Delta C/C_0$ of ~0.21% was achieved at a corresponding pressure load of 0.58 Pa, indicating that the as-fabricated sensor displayed high sensitivity that could sense extremely low pressures of < 1 Pa. Figure 5f shows the sensitivity plot of $\Delta C/C_0$ as a function of pressure. Considering that only the BNF@PDMS dielectric layer contributed to the $\Delta C/C_0$ relative to pressure, a remarkably high sensitivity of 0.854 kPa^{-1} at lower pressure range of up to ~0.5 kPa, and 0.29 kPa^{-1} for pressures ranging from ~0.55 to 2.1 kPa can be achieved for the BNF@PDMS based device. Further enhancements can be incorporated to render higher sensitivity of the device such as by micro-patterning the contact surface of the electrodes,[8b, 8c] or integration of high-*k* pores within the foam.[7b]

3. Conclusions

In summary, highly porous low-density BNF@PDMS were fabricated by coating diluted PDMS onto CVD grown few-layer *h*-BN foams. Importantly, the 3D interconnected network structure of *h*-BN enabled the conformal coating of diluted PDMS and acted as a supporting framework that prevented collapsing of the PDMS. Achieving densities as low as ~15 mg/cm^3, these BNF@PDMS are ~6 – 7 times lighter than lowest attainable PDMS foams to date. Moreover, the as-fabricated BNF@PDMS displayed remarkable mechanical resilience,

extremely high compressibility with good cyclic performance and superelastic properties. Owing to their high porosity, these foams also exhibited ultralow permittivity, close to that of air, and showed promising potential for multifunctional capacitive sensor applications. As demonstrated by a parallel-plate capacitive sensor using BNF@PDMS as a dielectric layer, various sensing capabilities were realized such as non-contact touch, environmental monitoring and high sensitivity pressure sensors.

4. Experimental Section

Synthesis of h-BN: *h*-BN growth was done *via* low pressure chemical vapor deposition (LPCVD) using Ni foams (2 mm thick, 100 PPI, Latech Scientific Supply Pte. Ltd.) as catalytic substrates. The Ni foam was first loaded into a 2-inch quartz tube furnace under a constant Ar/H_2 flow of 150/10 sccm at a pressure of 0.35 torr. The temperature of the furnace was ramped up to 1000 °C in 1 h and kept constant for another 2 h to anneal the Ni foam. To initiate *h*-BN growth, ~1.2 g of ammonia borane (97%, Sigma-Aldrich), which was placed in a ceramic boat outside the heating zone, was heated at ~120 – 150 °C using a heating belt. The growth was carried out for 1.5 h. After growth, the lid of the furnace was lifted for quick cooling and the sample was retrieved at room temperature.

Fabrication of BNF and BNF@PDMS: Diluted poly(methyl methacrylate) PMMA or poly(dimethylsiloxane) PDMS was first coated onto the as-grown BN/Ni foam to fabricate BNF and BNF@PDMS, respectively. For BNF, as-grown BN/Ni foam was first dip-coated in PMMA (PMMA-950-A4, MicroChem) and dried at ~80 °C for 1 h. For BNF@PDMS, PDMS (Sylgard 184 Silicone Elastomer, Dow Corning) solution of 3 – 10 wt% in *n*-hexane (99%, Sigma Aldrich) was first mixed using base part A and curing agent part B at a ratio of 10:1, followed by adding in a certain amount of *n*-hexane and ultrasonicated for 10 min. The as-grown BN/Ni foam was then immersed into the solution for 1 h and cured at ~80 °C overnight.

The PMMA or PDMS coated BN/Ni foam was then placed floating on diluted hydrochloric acid for 2 days to etch away the Ni foam. After completely etching the Ni, the PMMA/BN or PDMS/BN foam was then soaked in deionized (DI) water for a day to remove the acid residue. Finally, the PMMA/BN and PDMS/BN foams were dried in an oven at ~80 °C for several hours. To obtain free-standing BNF, PMMA/BN foam was further annealed under air at 700 °C for 3 h to remove the PMMA coating.

Fabrication of sensor: BNF@PDMS was used as the dielectric layer and indium tin oxide coated polyethylene terephthalate films (ITO/PETs) were used as conducting electrodes. The ITO/PETs were cut into 15 × 15 mm^2 and a Cu wire was attached onto the ITO surface using sliver paint. Two pieces of the ITO/PETs were then used to extract the BNF@PDMS out of the DI water with the ITO surfaces in contact to the BNF@PDMS. Finally, the entire stack was left to dry for several hours in the oven at ~80 °C.

Characterization: Scanning electron microscopy (SEM, JEOL JSM-IT100) was used to characterize the structural morphologies and SEM equipped with energy dispersive X-ray (EDX) analyzer (JEOL-7600F) was used to study the elemental composition of the various foams. Goniometer (Dataphysics OCA 25) was used to measure the contact angles of water and *n*-hexane on the surfaces of Ni and BN/Ni foams. High-resolution transmission electron microscopy (TEM, JEOL 2100F) was used to characterize the microstructure of BNF. Raman spectroscopy (WITEC CRM200 Raman system) was performed at room temperature using a 532 nm laser. Thermogravimetric analysis (TGA, Shimadzu DTG-60H thermal analyzer) was carried out on the various foams under a constant flow of air (100 mL/min) from 30 to 1000 °C at a heating rate of 10 °C/min. Uniaxial compression tests were performed using mechanical tester (Instron 5567) under ambient environment. The capacitance and dielectric properties of the various foams and sensors were measured using Keysight E4980 precision LCR meter. Varying compressive strains of the foams were tested using Keysight 16451B

dielectric test fixture controlled by a micromanipulator with an accuracy of 10 μm. A highly configurable force tester (ESM 303, Mark-10 Corporation) with a force gauge (Mark-10, Series 5) was used to apply external pressure for compression measurements on the sensor.

Supporting Information
Supporting Information is available from the Wiley Online Library or from the author.

Acknowledgements

R. Y. T. and H. L. contributed equally to this work.

Received: ((will be filled in by the editorial staff))
Revised: ((will be filled in by the editorial staff))
Published online: ((will be filled in by the editorial staff))

References

[1] a) C. Larson, B. Peele, S. Li, S. Robinson, M. Totaro, L. Beccai, B. Mazzolai, R. Shepherd, *Science* **2016**, *351*, 1071; b) S. Bauer, S. Bauer-Gogonea, I. Graz, M. Kaltenbrunner, C. Keplinger, R. Schwödiauer, *Adv. Mater.* **2014**, *26*, 149; c) X. Zhao, Q. Hua, R. Yu, Y. Zhang, C. Pan, *Adv. Electron. Mater.* **2015**, *1*, 1500142; d) X. Wang, L. Dong, H. Zhang, R. Yu, C. Pan, Z. L. Wang, *Adv. Sci.* **2015**, *2*, 1500169; e) J. Kim, M. Lee, H. J. Shim, R. Ghaffari, H. R. Cho, D. Son, Y. H. Jung, M. Soh, C. Choi, S. Jung, K. Chu, D. Jeon, S.-T. Lee, J. H. Kim, S. H. Choi, T. Hyeon, D.-H. Kim, *Nat. Commun.* **2014**, *5*, 5747; f) W. Honda, S. Harada, T. Arie, S. Akita, K. Takei, *Adv. Funct. Mater.* **2014**, *24*, 3299.

[2] a) D. Kwon, T.-I. Lee, J. Shim, S. Ryu, M. S. Kim, S. Kim, T.-S. Kim, I. Park, *ACS Appl. Mater. Interfaces* **2016**, *8*, 16922; b) S. G. Yoon, B. J. Park, S. T. Chang, *ACS Appl. Mater. Interfaces* **2017**, *9*, 36206; c) S. Wan, H. Bi, Y. Zhou, X. Xie, S. Su, K. Yin, L. Sun, *Carbon* **2017**, *114*, 209; d) S. Park, H. Kim, M. Vosgueritchian, S. Cheon, H. Kim, J. H. Koo, T. R. Kim, S. Lee, G. Schwartz, H. Chang, Z. Bao, *Adv. Mater.* **2014**, *26*, 7324.

[3] a) Y. Qin, Q. Peng, Y. Ding, Z. Lin, C. Wang, Y. Li, F. Xu, J. Li, Y. Yuan, X. He, Y. Li, *ACS Nano* **2015**, *9*, 8933; b) Y. R. Jeong, H. Park, S. W. Jin, S. Y. Hong, S.-S. Lee, J. S. Ha, *Adv. Funct. Mater.* **2015**, *25*, 4228; c) Z. Lou, S. Chen, L. Wang, K. Jiang, G. Shen, *Nano Energy* **2016**, 23, 7; d) Q. Liu, J. Chen, Y. Li, G. Shi, *ACS Nano* **2016**, *10*, 7901; e) C. Pang, G.-Y. Lee, T.-i. Kim, S. M. Kim, H. N. Kim, S.-H. Ahn, K.-Y. Suh, *Nat. Mater.* **2012**, *11*, 795.

[4] a) H. Zhong, J. Xia, F. Wang, H. Chen, H. Wu, S. Lin, *Adv. Funct. Mater.* **2017**, 27, 1604226; b) J.-H. Lee, H.-J. Yoon, T. Y. Kim, M. K. Gupta, J. H. Lee, W. Seung, H. Ryu, S.-W. Kim, *Adv. Funct. Mater.* **2015**, *25*, 3203.

[5] L. Lin, Y. Xie, S. Wang, W. Wu, S. Niu, X. Wen, Z. L. Wang, *ACS Nano* **2013**, *7*, 8266.

[6] M. Ramuz, B. C.-K. Tee, J. B.-H. Tok, Z. Bao, *Adv. Mater.* **2012**, *24*, 3223.

[7] a) S. C. B. Mannsfeld, B. C. K. Tee, R. M. Stoltenberg, C. V. H. H. Chen, S. Barman, B. V. O. Muir, A. N. Sokolov, C. Reese, Z. Bao, *Nat. Mater.* **2010**, *9*, 859; b) M. Pruvost, W. J. Smit, C. Monteux, P. Poulin, A. Colin, *npj Flexible Electron.* **2019**, *3*, 7; c) Z. He, W. Chen, B. Liang, C. Liu, L. Yang, D. Lu, Z. Mo, H. Zhu, Z. Tang, X. Gui, *ACS Appl. Mater. Interfaces* **2018**, *10*, 12816.

[8] a) Y. Joo, J. Byun, N. Seong, J. Ha, H. Kim, S. Kim, T. Kim, H. Im, D. Kim, Y. Hong, *Nanoscale* **2015**, *7*, 6208; b) T. Li, H. Luo, L. Qin, X. Wang, Z. Xiong, H. Ding, Y. Gu, Z. Liu, T. Zhang, *Small* **2016**, *12*, 5042; c) L. Ma, X. Shuai, Y. Hu, X. Liang, P. Zhu, R. Sun, C.-p. Wong, *J. Mater. Chem. C* **2018**, *6*, 13232.

[9] B. C. K. Tee, A. Chortos, R. R. Dunn, G. Schwartz, E. Eason, Z. Bao, *Adv. Funct. Mater.* **2014**, *24*, 5427.

[10] W. Hu, X. Niu, R. Zhao, Q. Pei, *Appl. Phys. Lett.* **2013**, *102*, 083303.

[11] C. Metzger, E. Fleisch, J. Meyer, M. Dansachmüller, I. Graz, M. Kaltenbrunner, C. Keplinger, R. Schwödiauer, S. Bauer, *Appl. Phys. Lett.* **2008**, *92*, 013506.

[12] H. Vandeparre, D. Watson, S. P. Lacour, *Appl. Phys. Lett.* **2013**, *103*, 204103.

[13] a) S. Kang, J. Lee, S. Lee, S. Kim, J.-K. Kim, H. Algadi, S. Al-Sayari, D.-E. Kim, D. Kim, T. Lee, *Adv. Electron. Mater.* **2016**, *2*, 1600356; b) S. Chen, B. Zhuo, X. Guo, *ACS Appl. Mater. Interfaces* **2016**, *8*, 20364.

[14] B. Su, S. Gong, Z. Ma, L. W. Yap, W. Cheng, *Small* **2015**, *11*, 1886.

[15] a) S.-J. Choi, T.-H. Kwon, H. Im, D.-I. Moon, D. J. Baek, M.-L. Seol, J. P. Duarte, Y.-K. Choi, *ACS Appl. Mater. Interfaces* **2011**, *3*, 4552; b) A. Zhang, M. Chen, C. Du, H. Guo, H. Bai, L. Li, *ACS Appl. Mater. Interfaces* **2013**, *5*, 10201.

[16] X. Zhao, L. Li, B. Li, J. Zhang, A. Wang, *J. Mater. Chem. A* **2014**, *2*, 18281.

[17] C. Yu, C. Yu, L. Cui, Z. Song, X. Zhao, Y. Ma, L. Jiang, *Adv. Mater. Interfaces* **2017**, *4*, 1600862.

[18] a) M. Chen, L. Zhang, S. Duan, S. Jing, H. Jiang, C. Li, *Adv. Funct. Mater.* **2014**, *24*, 7548; b) R. Ghosh, S. K. Reddy, S. Sridhar, A. Misra, *Carbon* **2016**, *96*, 439; c) H. Li, L. Jing, Z. L. Ngoh, R. Y. Tay, J. Lin, H. Wang, S. H. Tsang, E. H. T. Teo, *ACS Appl. Mater. Interfaces* **2018**, *10*, 41707.

[19] R. Zargar, J. Nourmohammadi, G. Amoabediny, *Biotechnol. Appl. Biochem.* **2016**, *63*, 190.

[20] a) M. Tebboth, Q. Jiang, A. Kogelbauer, A. Bismarck, *ACS Appl. Mater. Interfaces* **2015**, *7*, 19243; b) A. Kovalenko, K. Zimny, B. Mascaro, T. Brunet, O. Mondain-Monval, *Soft Matter* **2016**, *12*, 5154.

[21] X. Sun, X. Liu, X. Shen, Y. Wu, Z. Wang, J.-K. Kim, *Compos. Part A: Appl. Sci. Manuf.* **2016**, *85*, 199.

[22] a) T. Ouyang, Y. Chen, Y. Xie, K. Yang, Z. Bao, J. Zhong, *Nanotechnology* **2010**, 21, 245701; b) I. Jo, M. T. Pettes, J. Kim, K. Watanabe, T. Taniguchi, Z. Yao, L. Shi, *Nano Lett.* **2013**, *13*, 550.

[23] a) L. Song, L. Ci, H. Lu, P. B. Sorokin, C. Jin, J. Ni, A. G. Kvashnin, D. G. Kvashnin, J. Lou, B. I. Yakobson, P. M. Ajayan, *Nano Lett.* **2010**, *10*, 3209; b) S. M. Kim, A. Hsu, M. H. Park, S. H. Chae, S. J. Yun, J. S. Lee, D.-H. Cho, W. Fang, C. Lee, T. Palacios, M. Dresselhaus, K. K. Kim, Y. H. Lee, J. Kong, *Nature Commun.* **2015**, *6*, 8662.

[24] a) Z. Liu, Y. Gong, W. Zhou, L. Ma, J. Yu, J. C. Idrobo, J. Jung, A. H. MacDonald, R. Vajtai, J. Lou, P. M. Ajayan, *Nat. Commun.* **2013**, *4*, 2541; b) L. H. Li, J. Cervenka, K. Watanabe, T. Taniguchi, Y. Chen, *ACS Nano* **2014**, *8*, 1457.

[25] a) Q. Weng, B. Wang, X. Wang, N. Hanagata, X. Li, D. Liu, X. Wang, X. Jiang, Y. Bando, D. Golberg, *ACS Nano* **2014**, *8*, 6123; b) L. Jing, H. Li, R. Y. Tay, B. Sun, S. H. Tsang, O. Cometto, J. Lin, E. H. T. Teo, A. I. Y. Tok, *ACS Nano* **2017**, *11*, 3742.

[26] J. Yin, X. Li, J. Zhou, W. Guo, *Nano Lett.* **2013**, *13*, 3232.

[27] a) C. Y. Hui, A. Jagota, Y. Y. Lin, E. J. Kramer, *Langmuir* **2002**, *18*, 1394; b) K. G. Sharp, G. S. Blackman, N. J. Glassmaker, A. Jagota, C.-Y. Hui, *Langmuir* **2004**, *20*, 6430; c) Y. Xue, D. Kang, Y. Ma, X. Feng, J. A. Rogers, Y. Huang, *Extreme Mech. Lett.* **2017**, *11*, 18.

[28] R. V. Gorbachev, I. Riaz, R. R. Nair, R. Jalil, L. Britnell, B. D. Belle, E. W. Hill, K. S. Novoselov, K. Watanabe, T. Taniguchi, A. K. Geim, P. Blake, *Small* **2011**, *7*, 465.

[29] D. Cai, A. Neyer, R. Kuckuk, H. M. Heise, *J. Mol. Struct.* **2010**, *976*, 274.

[30] Y. Xue, P. Dai, M. Zhou, X. Wang, A. Pakdel, C. Zhang, Q. Weng, T. Takei, X. Fu, Z. I. Popov, P. B. Sorokin, C. Tang, K. Shimamura, Y. Bando, D. Golberg, *ACS Nano* **2017**, *11*, 558.

[31] K. K. Kim, A. Hsu, X. Jia, S. M. Kim, Y. Shi, M. Dresselhaus, T. Palacios, J. Kong, *ACS Nano* **2012**, *6*, 8583.

[32] J. Brandrup, E. H. Immergut, E. A. Grulke, *PolymerHandbook*, 4th ed., Wiley, New York, **2003**.

[33] M. Kang, J. Kim, B. Jang, Y. Chae, J.-H. Kim, J.-H. Ahn, *ACS Nano* **2017**, *11*, 7950.

[34] J. M. Choi, T. W. Kim, *Trans. Elect. Electron. Mater.* **2013**, *14*, 182.

[35] B. T. Cooke, J. Julicher, K. Curtis, *US Patent 8,884,771 B2* **2014**.

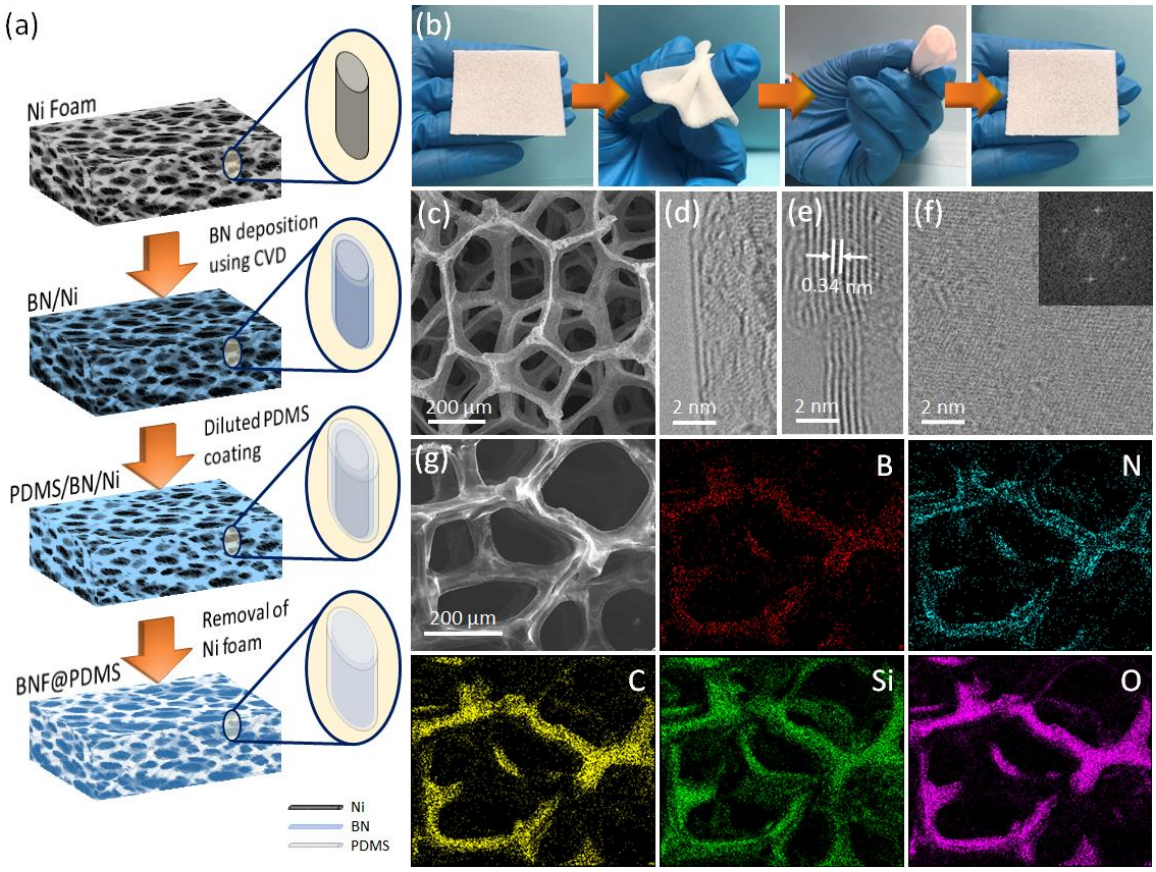

Figure 1. (a) Schematic of the fabrication process of BNF@PDMS. (b) Photographs of the recovery sequence of BNF@PDMS undergoing various deformations such as bending, twisting and rolling. (c) SEM image of a free-standing BNF. Atomic resolution TEM images taken at the (d,e) folded edges and (f) within the interior of few-layer *h*-BN sheets. The inset in (f) shows its corresponding fast Fourier transform (FFT). (g) SEM image and its corresponding EDX elemental mappings of the BNF@PDMS.

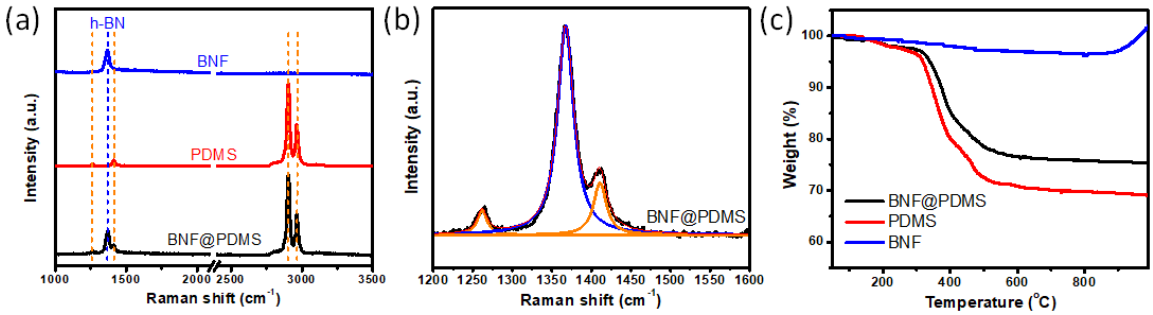

Figure 2. (a,b) Raman and (c) TGA spectra of pure BNF, pure PDMS foam and BNF@PDMS.

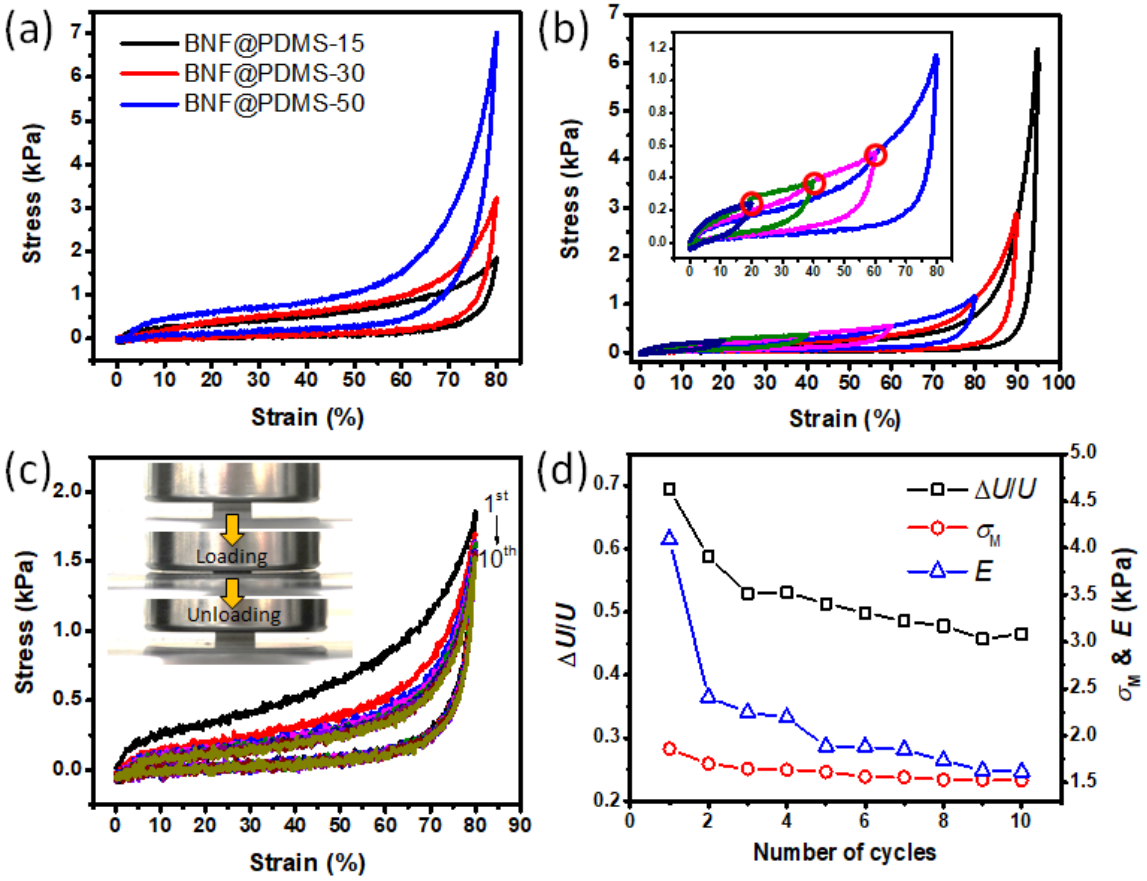

Figure 3. (a) σ–ε curves of BNF@PDMS with various densities of 15 (black trace), 30 (red trace) and 50 mg/cm^3 (blue trace) at 80% strain amplitude. (b) Sequential loading-unloading cycles of BNF@PDMS-15 from 20% to 95% strain amplitudes. The inset shows a magnified plot of (b) up to 80% strain. The red circles indicate the intersection points between the preceding and successive σ–ε curves. (c) Cyclic compression tests of BNF@PDMS-15 at 80% strain amplitude. The inset shows the sequential photographs of BNF@PDMS-15 undergoing a load-unloading cycle. (d) Summary plots of the energy loss coefficients ($\Delta U/U$), maximum compressive stress (σ_M), and elastic modulus (E) extracted from the 10 compression cycles.

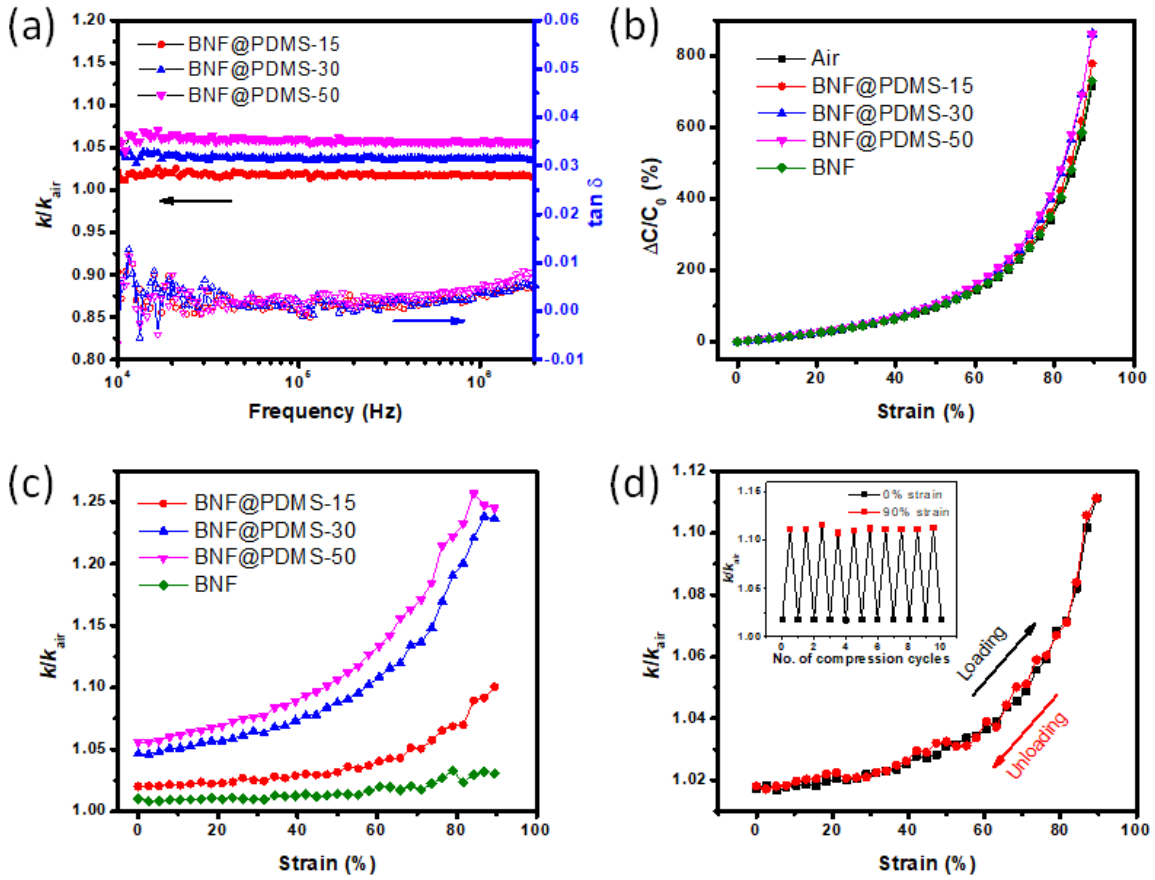

Figure 4. (a) Plots of the dielectric constant relative to air (k/k_{air}) and loss tangent (tan δ) as a function of frequency and (b) change in capacitance ($\Delta C/C_0$) and (c) k/k_{air} as a function of strain for BNF@PMDS-15 (red trace), BNF@PDMS-30 (blue trace), BNF@PDMS-50 (magenta trace), BNF (green trace) and air (black trace). (d) Evolution of k/k_{air} as a function of strain during the first compression cycle at 90% strain for BNF@PDMS-15. The inset shows the change in k/k_{air} at 0 and 90% strains for 10 consecutive compression cycles.

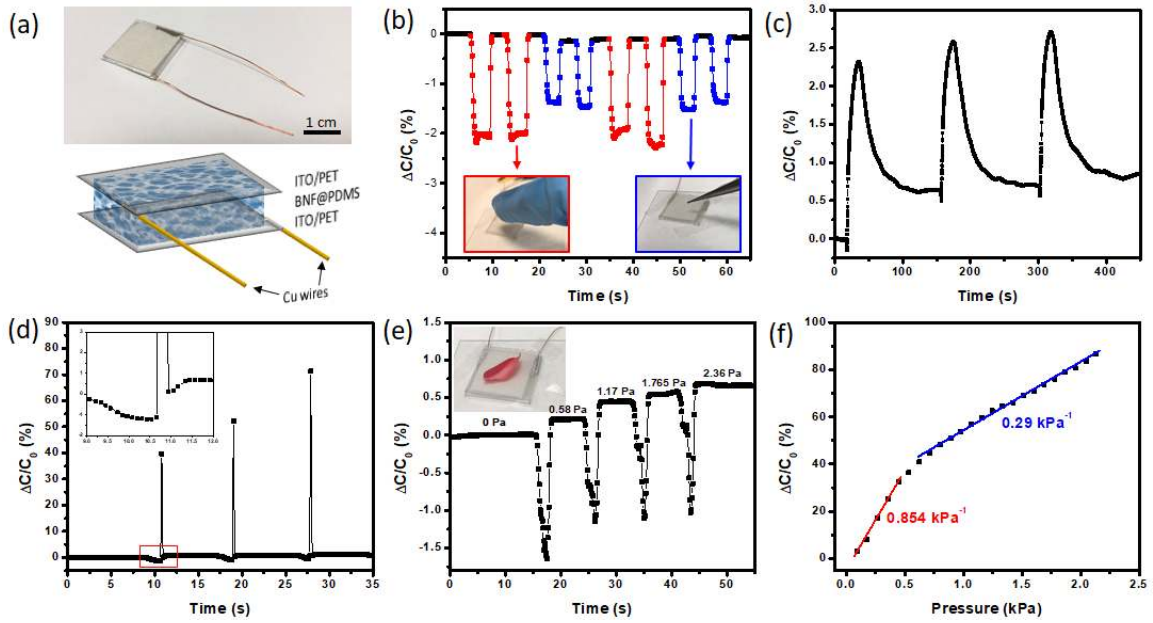

Figure 5. (a) Photograph (top) and schematic (bottom) of a parallel-plate capacitive sensor using ITO/PETs as the conducting electrodes and BNF@PDMS as the dielectric layer. Plots of $\Delta C/C_0$ as a function of applied (b) non-contact touch by hovering a finger (red) and a tweezer (blue) at close proximity to the device, and (c) environmental change by gently blowing through the device. The insets in (b) shows the photographs of a hovering finger (boxed in red) and tweezer (boxed in blue) on top of the device. Plots of $\Delta C/C_0$ as a function of applied pressure by (d) pressing onto the device with a tweezer for three times with increasing intensity, and (e) loading a total of four flower petals in successive sequence. The inset in (d) shows the initial dip in $\Delta C/C_0$ prior to the spike which was activated by the pressing motion. The inset in (e) shows a photograph of a flower petal placed on top of the device. (f) Pressure-response curve of the sensor displaying its sensitivity from 0 – 2.1 kPa.

Boron nitride (BN) foams were used as frameworks to produce the lightest polydimethylsiloxane (PDMS)-based foams to date with densities reaching as low as 15 mg/cm^3. The BN/PDMS composite foams (BNF@PDMS) displayed excellent mechanical resilience, extremely high compressibility and superelastic properties. Owing to these unique properties, the BNF@PMDS showed great potential as a dielectric layer for multifunctional capacitive sensor applications.

Dielectrics

*Roland Yingjie Tay, Hongling Li, Jinjun Lin, Hong Wang, Jacob Song Kiat Lim, Shuai Chen, Wei Lin Leong, Siu Hon Tsang, and Edwin Hang Tong Teo**

Lightweight, Superelastic Boron Nitride/Polydimethylsiloxane Foam as Air Dielectric Substitute for Multifunctional Capacitive Sensor Applications

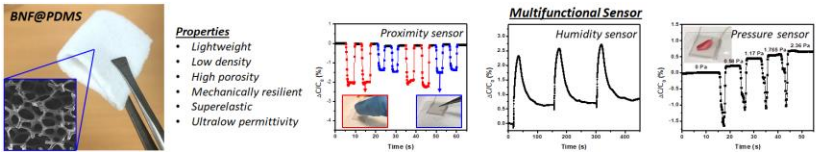

Supporting Information

Lightweight, Superelastic Boron Nitride/Polydimethylsiloxane Foam as Air Dielectric Substitute for Multifunctional Capacitive Sensor Applications

*Roland Yingjie Tay, Hongling Li, Jinjun Lin, Hong Wang, Jacob Song Kiat Lim, Shuai Chen, Wei Lin Leong, Siu Hon Tsang, and Edwin Hang Tong Teo**

Dr. R. Y. Tay, Dr. H. Li, J. Lin, Dr. H. Wang, Dr. S. Chen, Prof. W. L. Leong, Prof. E. H. T. Teo
School of Electrical and Electronic Engineering, Nanyang Technological University, 50 Nanyang Avenue, Singapore 639798, Singapore
E-mail: htteo@ntu.edu.sg

Dr. R. Y. Tay, J. S. K. Lim, Dr. S. H. Tsang
Temasek Laboratories@NTU, 50 Nanyang Avenue, Singapore 639798, Singapore

J. S. K. Lim, Prof. E. H. T. Teo
School of Materials Science and Engineering, Nanyang Technological University, 50 Nanyang Avenue, Singapore 639798, Singapore

Table S1. List of the various foam densities obtained using different PDMS concentrations.

Foam	Wt% of PDMS	ρ (mg/cm^3)
BNF	0%	0.90 ± 0.1
BNF@PDMS	3%	15.25 ± 2.1
BNF@PDMS	5%	30.86 ± 2.5
BNF@PDMS	10%	49.96 ± 3.3

Table S2. Properties of various foam-like materials.

Material	ρ (mg/cm^3)	ε_M (%)	σ_M	E (kPa)	Ref.
BN/PDMS	**~15**	**95**	**1.86 kPa @ 80%strain**	**4.12**	**This work**
Polyolefin	~330				[1]
Polyurethane	100 – 400				[2]
PDMS	100				[3]
PDMS	120 – 420				[4]
PDMS	200 – 600				[5]
PDMS	180 – 750				[6]
PDMS	640 – 960				[7]
PDMS	816	60	~16 MPa @ 60% strain		[8]
Graphene/PDMS	869	70	~37.44 MPa @ 80% strain		[8]
Graphene/PDMS	27.2 – 69.2	95	~0.1 MPa @ 80% strain	0.15	[9]
Graphene/PDMS	90 – 880				[10]
BN	5.3 – 8.2	50	~1.25 kPa @ 50% strain	6	[11]
BN	1.6	70	70 Pa @ 70% strain	0.127	[12]
BN	1.4				[13]
Graphene	~5				[14]
Graphene	9.6 – 32				[15]
Graphene	~10				[16]
Graphene	0.18 – 50	12	1.1 kPa @ 12% strain	15	[17]
Graphene	5.1	80	18.55 kPa @ 80% strain	20	[18]
Graphene	~5.5		~13 kPa @ 50% strain	~89	[19]
Graphene/PI	10	50	~2.5 kPa @ 50% strain	3	[20]
Graphene/CNT	14	80	~300 kPa @ 80% strain	750	[21]
CNT	5 – 10	80	50 kPa @ 80% strain	140	[22]
GO	4.8	50	~5 kPa @ 50% strain	8.2	[23]

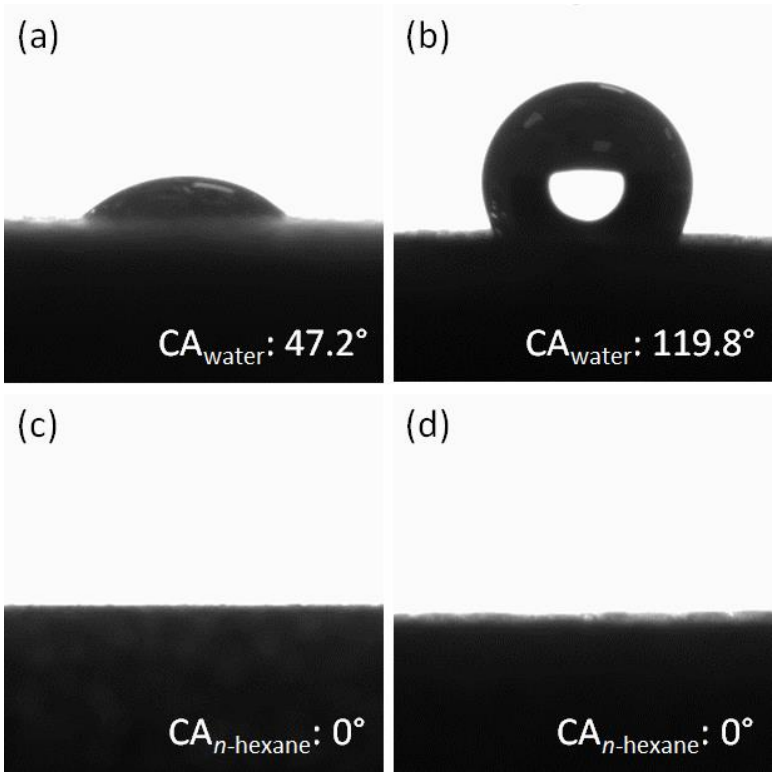

Figure S1. Contact angle (CA) measurements using (a,b) water and (c,d) *n*-hexane on Ni and BN/Ni foam, respectively.

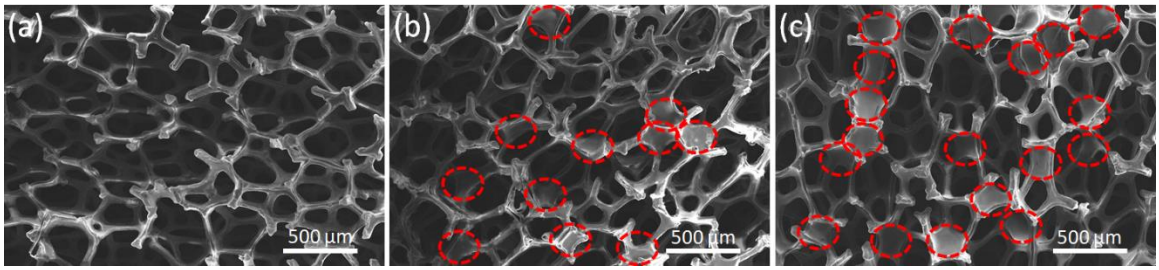

Figure S2. SEM images of BNF@PDMS foams using (a) 3, (b) 5 and (c) 10 wt% PDMS coating solution. The red dashed circles indicate covered pores due to higher concentration of PDMS used for coating solution.

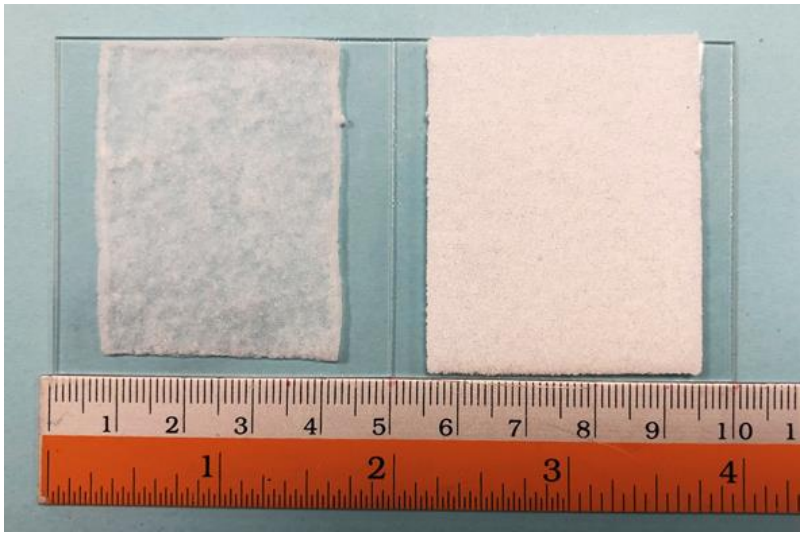

Figure S3. Photograph of a highly uneven collapsed PDMS foam (left) and a BNF@PDMS foam with a well-preserved structure (right) using the same 3 wt% PDMS coating solution.

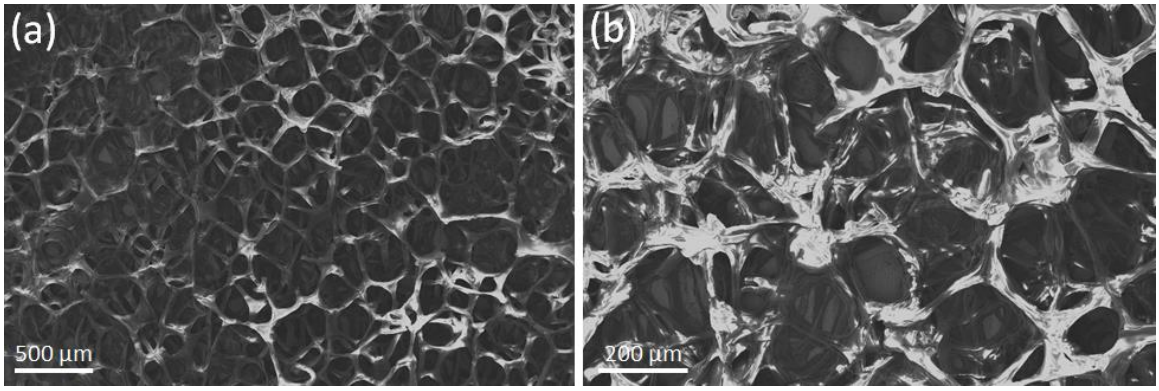

Figure S4. (a) SEM and (b) magnified SEM images of the collapsed PDMS foam with uneven struts.

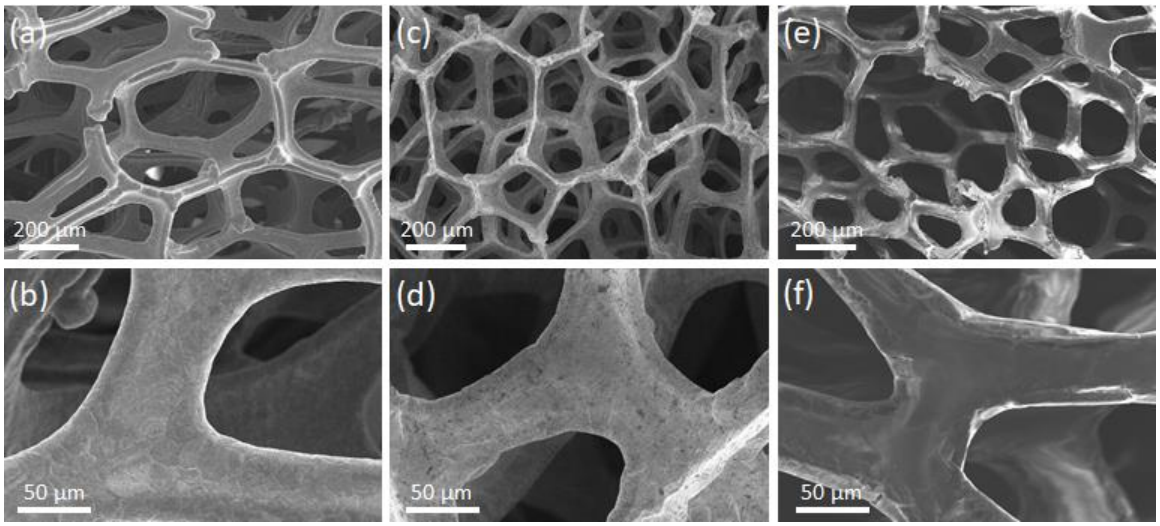

Figure S5. SEM and magnified SEM images of (a,b) as-grown BN on Ni foam, (c,d) freestanding BNF and (e,f) BNF@PDMS.

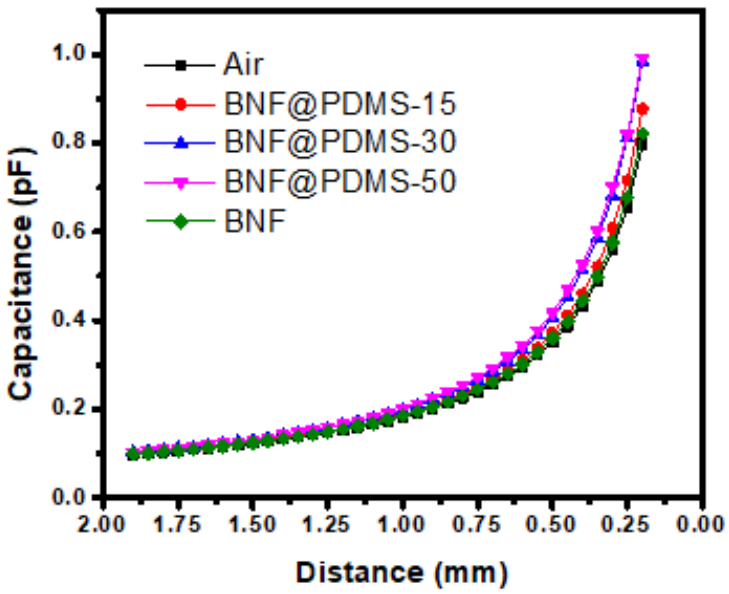

Figure S6. Plot of capacitance as a function of distance of the various foams.

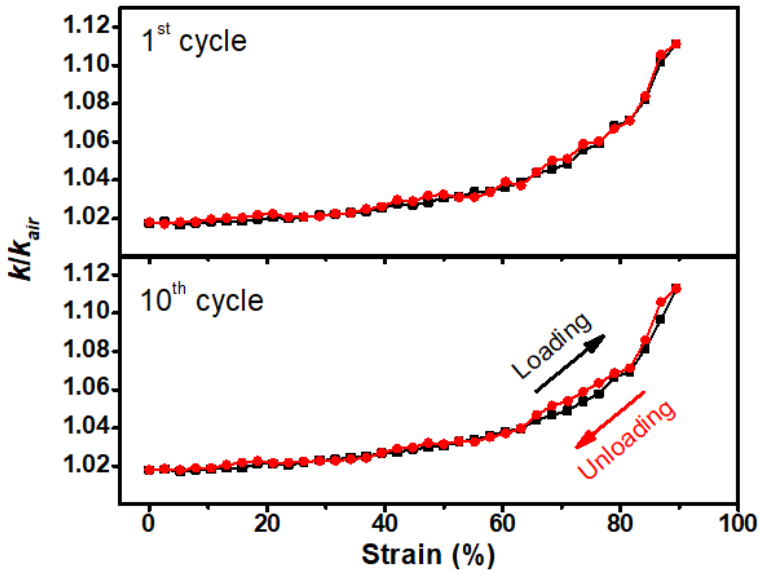

Figure S7. Evolution of k/k_{air} as a function of strain during the first and tenth compression cycle at 90% strain for BNF@PDMS-15.

References

[1] C. Metzger, E. Fleisch, J. Meyer, M. Dansachmüller, I. Graz, M. Kaltenbrunner, C. Keplinger, R. Schwödiauer, S. Bauer, *Appl. Phys. Lett.* **2008**, *92*, 013506.

[2] H. Vandeparre, D. Watson, S. P. Lacour, *Appl. Phys. Lett.* **2013**, *103*, 204103.

[3] M. Chen, L. Zhang, S. Duan, S. Jing, H. Jiang, C. Li, *Adv. Funct. Mater.* **2014**, *24*, 7548.

[4] A. Zhang, M. Chen, C. Du, H. Guo, H. Bai, L. Li, *ACS Appl. Mater. Interfaces* **2013**, *5*, 10201.

[5] C. Yu, C. Yu, L. Cui, Z. Song, X. Zhao, Y. Ma, L. Jiang, *Adv. Mater. Interfaces* **2017**, *4*, 1600862.

[6] S.-J. Choi, T.-H. Kwon, H. Im, D.-I. Moon, D. J. Baek, M.-L. Seol, J. P. Duarte, Y.-K. Choi, ACS *Applied Materials & Interfaces* **2011**, *3*, 4552.

[7] A. D. Lantada, H. A. Iniesta, B. P. Sanchez, J. P. Garcia, *Adv. Mater. Sci. Eng.* **2014**, *2014*, 612976.

[8] R. Ghosh, S. K. Reddy, S. Sridhar, A. Misra, *Carbon* **2016**, *96*, 439.

[9] H. Li, L. Jing, Z. L. Ngoh, R. Y. Tay, J. Lin, H. Wang, S. H. Tsang, E. H. T. Teo, ACS *Appl. Mater. Interfaces* **2018**, *10*, 41707.

[10] X. Sun, X. Liu, X. Shen, Y. Wu, Z. Wang, J.-K. Kim, *Compos. Part A: Appl. Sci. Manuf.* **2016**, *85*, 199.

[11] J. Wang, D. Liu, Q. Li, C. Chen, Z. Chen, P. Song, J. Hao, Y. Li, S. Fakhrhoseini, M. Naebe, X. Wang, W. Lei, *ACS Nano* **2019**, *13*, 7860.

[12] J. Yin, X. Li, J. Zhou, W. Guo, *Nano Lett.* **2013**, *13*, 3232.

[13] W. Lei, V. N. Mochalin, D. Liu, S. Qin, Y. Gogotsi, Y. Chen, *Nat. Commun.***2015**, *6*, 8849.

[14] Z. Chen, W. Ren, L. Gao, B. Liu, S. Pei, H.-M. Cheng, *Nat. Mater.* **2011**, *10*, 424.

[15] M. T. Pettes, H. Ji, R. S. Ruoff, L. Shi, *Nano Lett.* **2012**, *12*, 2959.

[16] M. A. Worsley, P. J. Pauzauskie, T. Y. Olson, J. Biener, J. H. Satcher, T. F. Baumann, *J. Am. Chem. Soc.* **2010**, *132*, 14067.

[17] M. Mecklenburg, A. Schuchardt, Y. K. Mishra, S. Kaps, R. Adelung, A. Lotnyk, L. Kienle, K. Schulte, *Adv. Mater.* **2012**, *24*, 3486.

[18] L. Qiu, J. Z. Liu, S. L. Y. Chang, Y. Wu, D. Li, *Nat. Commun.* **2012**, *3*, 1241.

[19] Y. A. Samad, Y. Li, S. M. Alhassan, K. Liao, *ACS Appl. Mater. Interfaces* **2015**, *7*, 9195.

[20] Y. Qin, Q. Peng, Y. Ding, Z. Lin, C. Wang, Y. Li, F. Xu, J. Li, Y. Yuan, X. He, Y. Li, *ACS Nano* **2015**, *9*, 8933.

[21] K. H. Kim, Y. Oh, M. F. Islam, *Nat. Nanotechnol.* **2012**, *7*, 562.

[22] X. Gui, J. Wei, K. Wang, A. Cao, H. Zhu, Y. Jia, Q. Shu, D. Wu, *Adv. Mater.* **2010**, *22*, 617.

[23] S. Wan, H. Bi, Y. Zhou, X. Xie, S. Su, K. Yin, L. Sun, *Carbon* **2017**, *114*, 209.